Meteorological Society of Japan

Journal of the Meteorological Society of Japan, Vol. 74, No. 4, pp. 493–508, 1996

Maturing Process of the Summer Monsoon over the Western North Pacific — A Coupled Ocean/Atmosphere System —

By Hiroaki Ueda and Tetsuzo Yasunari

Institute of Geoscience, University of Tsukuba, Tsukuba, Ibaraki 305, Japan

(Manuscript received 5 February 1996, in revised form 8 June 1996)

Abstract

The abrupt northward shift of the active convective region from 10°N to 25°N around 150°E on July 25–29 (Pentad 42) seen in the seasonal cycle of the summer monsoon over the western North Pacific (convection jump) and other associated phenomena preceding this convection jump are investigated using data of equivalent black body temperature derived from GMS and sea surface temperature (SST) for the period of 1980–1994 together with circulation field data objectively analyzed by the ECMWF.

The mechanism of the maturing process of the summer monsoon between middle June and late July are examined by comparing 8-year remarkable convection jump years (typical cases) and other years (atypical cases). Tongue-shaped warm-SST areas (warmer than 29°C) are observed in early July around 20°N, 150–160°E, preceding the typical convection jump. This warming of SST is closely related to the appearance of a weak-wind region (weakening of easterlies) around 25°N, 140°E–160°E in late June. These weak easterlies are likely to be associated with the propagation of a Rossby wave induced by the occurrence of the active convection near the Philippine Islands in middle to late June. Most of the atypical cases appear in the El-Niño years.

1. Introduction

The seasonal changes of large-scale convective activity and circulation field over the western North Pacific are largely modulated by an ocean-land-atmosphere interaction, in spite of the simple annual cycle forcing of solar radiation (Matsumoto, 1989, 1990, 1992; Nakazawa, 1992; Tanaka, 1992; Murakami and Matsumoto, 1994; Ueda, Yasunari and Kawamura, 1995). Ueda *et al.* (1995) showed that the sudden onset of the summer monsoon over the subtropical western North Pacific in late July is associated with an abrupt northward shift of enhanced convection over 20°N, 150°E. In the present study we call this phenomenon a "convection jump". At the same time, the withdrawal of the Baiu season around Japan occurs drastically as a result of the northward shift of the Baiu front associated with the Rossby-wave propagation generated by the atmospheric heat source of this convection jump.

However, the mechanism of the convection jump and its interannual variability are not fully understood yet, since the results of Ueda *et al.* (1995) were investigated based on mean climatological data. Ueda *et al.* (1995) suggested that an appearance of a warm SST (sea surface temperature) pool in excess of 29°C in early July over the region of the convection jump, coupled with the seasonal evolution of the Pacific subtropical high system, is one of the important factors for the creation of a convection jump.

In this paper, we further focus on this process which is particularly relevant to the interannual variation of the convection jump. We document data in Section 2, describe the interannual variation of the convection jump in Section 3, and discuss the correlation between the SST and the interannual variability of the convection jump in Section 4. In this section, a composite analysis is carried out to reveal the spatial distribution of the SST based on the correlation analysis. In addition, a detailed description of the atmospheric instability associated with the SST warming is also presented. In Section 5, we examine the association between the SST and the behavior of the Pacific high as a seasonal evolution. Furthermore, the relationship between the appearance of the active convective activity around the Philippine Islands in middle June and the variation of the western part of the Pacific high is investigated. In Section 6, the whole maturing process of the summer monsoon over the western North Pacific is summarized as a schematic model presenting the onset of the active tropical western Pacific monsoon

©1996, Meteorological Society of Japan

NACSIS-Electronic Library Service

Meteorological Society of Japan

in middle June, followed by the convection jump in late July as an atmosphere-ocean interaction. The conclusions are summarized in Section 7.

2. Data

One degree longitude-latitude mesh mean data of the infrared equivalent black body temperature observed from GMS (T_{BB}), three-hourly for the period 1980–1994, are utilized in the present study as a measure of large-scale convection over tropical and subtropical regions. Pressure and wind field data objectively analyzed by ECMWF, twice-daily for the period 1980–1989, are partly used to examine the situation of circulation fields. Ten-day means of sea surface temperature (SST) collected by the JMA for the period 1980–1994 are also utilized to examine the relation with the convection.

3. T_{BB} and wind fields

As already noted in Ueda *et al.* (1995), the abrupt northward shift of large-scale convective activity (convection jump) in the climatological mean (1980–1989) T_{BB} field occurs at Pentad 42 (July 25-July 29) around 15°N–25°N, 150°E–160°E, which we call the "key region". In this section the interannual variation of the convection jump is examined and the jumps are classified into two groups, "typical case" and "atypical case" of the convection jump to perform a composite analysis. The definition of typical cases is expressed as

$$T_{BB}(i, P42-43) < 260\ K, \tag{1}$$

where i means the i-th year from 1980 and $P42$–43 averaged over Pentads 42 through 43. If T_{BB} (i, $P42$–43) does not satisfy condition (1), we consider it an atypical case. Using (1), the years 1980, 1981, 1984, 1985, 1988, 1989, 1990 and 1994 are typical cases and the years 1982, 1983, 1986, 1987, 1991, 1992 and 1993 are the atypical cases.

Time series of T_{BB} are made for (a) typical cases, and (b) atypical cases from Pentad 30 (May 26–May 30) to Pentad 60 (Oct. 23–Oct. 27), as shown in Fig. 1. In this figure, the thick line represents the mean series of typical cases and atypical cases, respectively. The seasonal change of mean typical cases (upper panel) reveals a remarkable minimum at Pentad 42 (250 K) and a secondary minimum at Pentad 46 (260 K) which indicate the occurrences of enhanced convection at these periods, while in the atypical cases (lower panel), this minimum of T_{BB} at Pentad 42 can not be recognized. A weak minimum (more than 270 K) is found from Pentad 45 to Pentad 47 (Aug. 9–Aug. 23), that is to say, active convection does not appear around late July but preferably appears in the middle of August with less T_{BB} intensity and a larger variability.

The composite T_{BB} and wind fields at Pentad 42 were produced for the typical and atypical cases. The horizontal distributions of T_{BB} and wind fields at 850 hPa for (a) typical cases and (b) atypical cases are shown in Fig. 2. In Fig. 2a the most enhanced convection with a T_{BB} of less than 250 K appear both around the Philippine Islands and the north western Pacific around 20°N, 150°E. The warmer T_{BB} values of less than 270 K occur in the belt extending between the two regions of the active convection. In the wind field, the southwest monsoon flows from southeast Asia across over the Philippines, expands eastward to 150°E, and then merges with the easterlies from the central Pacific to produce southeasterlies with cyclonic wind shear. In contrast, convective activity is weak for atypical cases around the key region, while the center of the active convection is seen around 10°N (Fig. 2b). The monsoon westerlies are not observed to the east of the Philippines. On the other hand, the easterly wind dominates east of 130°E along the northern periphery of the low T_{BB} area of less than 270 K.

4. Sea surface temperature

Based on the climatological mean SST data, Ueda *et al.* (1995) indicated that a warm SST pool exceeding 29°C over the key region in early July is likely to be one important necessary condition for the convection jump. In this section, we examine the relationship between the convection jump and seasonal changes of SST over the same area in terms of interannual variability.

A longitude–time section of correlation coefficients between the T_{BB} (i, $P42$–43) of the key region and the SST (i, J) of the same latitudes is shown in Fig. 3, where i represents the SST of each year averaged between 15°N and 25°N and J denotes the 10-day mean SST. In this figure, a negative (positive) correlation means that a positive (negative) SST anomaly is correlated to active (inactive) convection in late July. The most prominent feature seen in Fig. 3 is a large negative correlation around early to middle July between 150°E and 165°E. The year-to-year variations of T_{BB} (i, $P42$–43) and SST (i, J) at 158°E in middle July, as shown in Fig. 4, clearly demonstrates a high correlation between T_{BB} (i, $P42$–43) and SST (i, J) with a coefficient of 0.81. These two figures indicate that when the SST is warmer (colder) over the key region in the half first of July then a convection jump occurs (does not occur) there 10–20 days later. Another intriguing feature in Fig. 3 is the positive correlation coefficients observed around early August over the region of the convection jump, which indicates that SST decreases after the enhancement of the convection, presumably because of a decrease of solar radiation on account of the existence of convective clouds, as well as strong evaporative cooling and turbulent mixing between the warm sea surface water and the underlying cold water due to strengthening wind speed.

NACSIS-Electronic Library Service

Meteorological Society of Japan

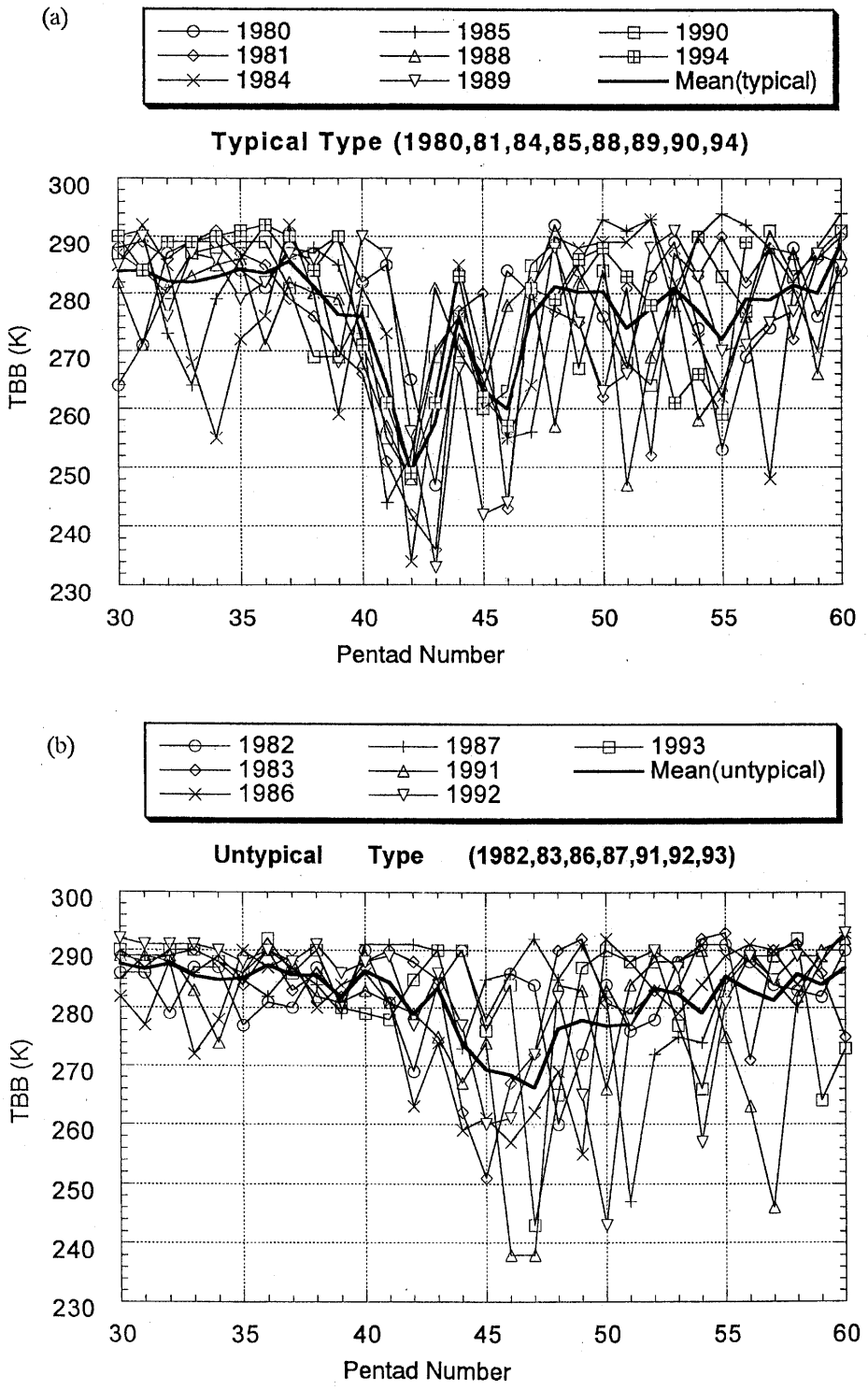

Fig. 1. Time series of Pentad mean T_{BB} in the key region (15°N–25°N, 150°E–160°E) for the period from Pentad 30 to Pentad 60. (a) Typical cases (1980, 81, 84, 85, 88, 89, 90, 94), (b) atypical cases (1982, 83, 86, 87, 91, 92, 93).

Next, we examine the horizontal distribution of SST in early July both for the typical and the atypical cases of the convection jump. Figure 5 represents the composited SST in early July for (a) typical cases, and (b) atypical cases. Both in Figs. 5a and 5b, a warm SST pool of more than 29°C is observed between the equator and 20°N and 110°E to 150°E. The warmest condition with more than 29.5°C is seen between 10°N and 20°N. It is interesting to note that a warm SST tongue extends eastward along 20°N over the key region for typical cases. By subtracting the composite for atypical

NACSIS-Electronic Library Service

Meteorological Society of Japan

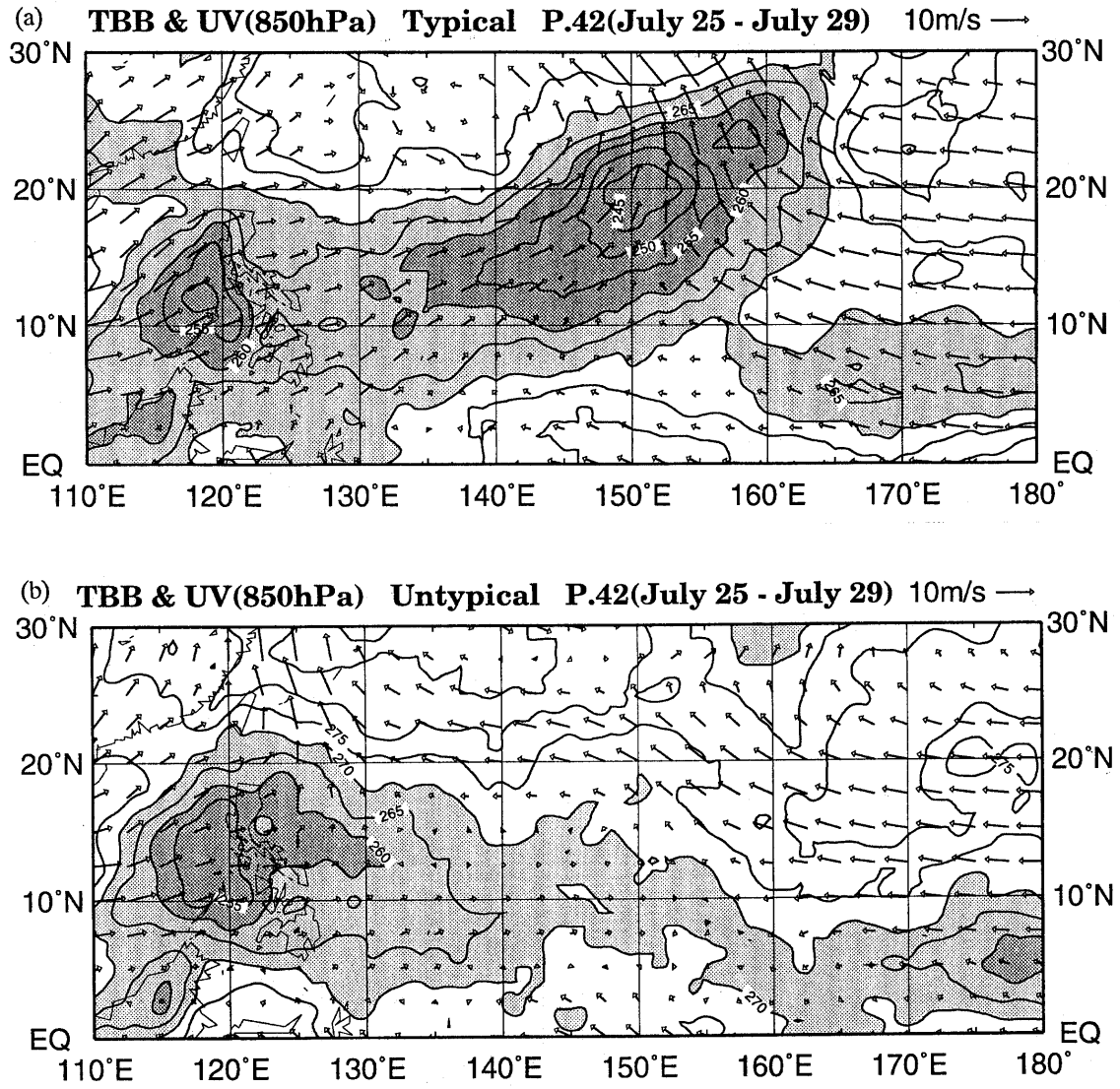

Fig. 2. Composite of T_{BB} and 850 hPa wind at Pentad 42 (July 25–30) for (a) typical cases, (b) atypical cases. The contour interval is 5 K. Heavy shading denotes areas with T_{BB} less than 260 K, while light shading is for areas between 260 K and 270 K. A scale vector is shown at the upper-right of each figure.

cases from that for typical cases, positive anomalies exceeding 0.4°C are elongated zonally east beyond 150°E along 20°N (Fig. 5c), which corresponds to the low T_{BB} region in late July of typical cases (see Fig. 2a). Another interesting feature is the existence of negative anomalies to the northeast of the Philippine Islands around 15°N, 130°E, which is concurrent with inactive convection for the typical cases over the same region. These contrasting features in both SST and T_{BB} anomalies indicate that when the SST is warmer (colder) than usual over the key region then convection becomes active (inactive) with 10–20 days time lag.

Gadgil *et al.* (1984) indicated that convection becomes active when the SST rises to greater than 28 to 29°C over the tropical ocean. Ueda *et al.* (1995) showed that the SST over the key region is warmer than 29°C in early July. However, the convection jump occurs in late July, about 20 days later. The question arises: How has the stability of the atmosphere changed during these 20 days? In the present study, the atmospheric moist instability is investigated using the equivalent potential temperature of a saturated parcel, given by

$$\theta e = \theta \exp(L_c q_s / C_p T). \quad (2)$$

Here θ is the potential temperature, L_c is latent

NACSIS-Electronic Library Service

Meteorological Society of Japan

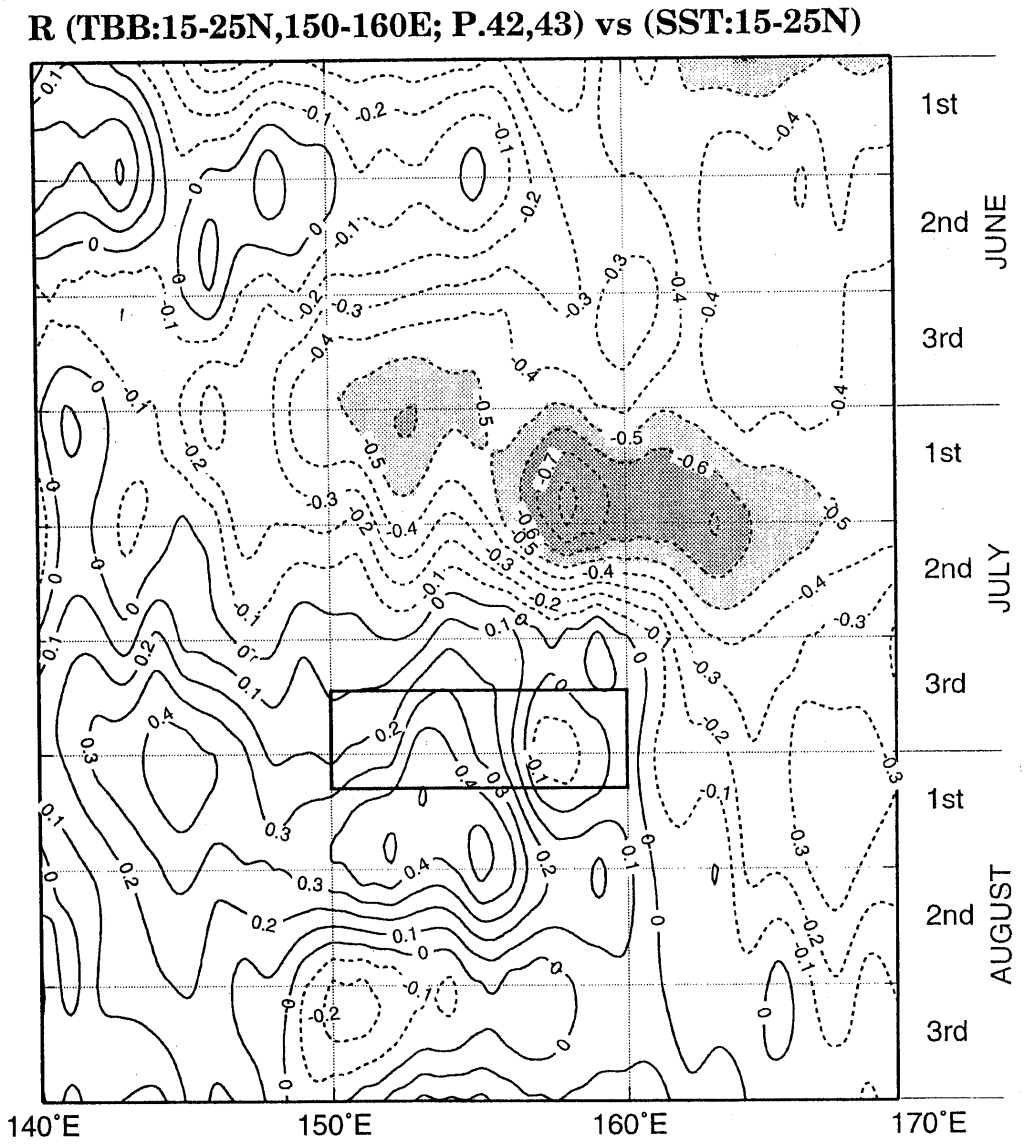

Fig. 3. Time-longitude sections of correlation coefficients between interannual variation of T_{BB} in the key region (15°N–25°N, 150°E–160°E) during Pentads 42, 43 (July 25–August 3) and the interannual variation of SST averaged over the same latitudes. Intervals are 0.1, with shading (dark shading) indicating regions of less than −0.5 (−0.6). The reference T_{BB} is shown as a solid square.

heat of condensation, q_s is saturation mixing ratio, T is temperature and C_p is the specific heat of dry air. Thus the conditional stability criterion for a saturated parcel is

$$\frac{\partial \theta_e}{\partial_p} = \begin{cases} < 0 & \text{conditionally unstable,} \\ = 0 & \text{saturated neutral,} \\ > 0 & \text{conditonally stable.} \end{cases} \quad (3)$$

In this study, we focus on the vertical gradient of θ_e of the low-level atmosphere between 1000 hPa and 850 hPa. Figure 6 shows time changes of equivalent potential temperature gradient for typical cases from Pentad 36 (June 25–June 29) to Pentad 42 (July 25–July 29) at every other pentad. The hatched area is considered to be a strong conditionally unstable region. In these time sequences, the atmosphere becomes unstable from late June to early July over the region of 15°N–25°N, 135°E–155°E. The most unstable condition over the above region at Pentad 38 corresponds well with the warm SST tongue warmer than 29°C in early July (see Fig. 5a and Fig. 11b of Ueda *et al.* (1995)). After that, the unstable condition is reduced from Pentads 40 to 42, which is coincident with the timing of the generation of the convection (convection jump). These results indicate that the atmosphere becomes most unstable over the key region in early July due to the warming of a high SST. In the subsequent 10

NACSIS-Electronic Library Service

Meteorological Society of Japan

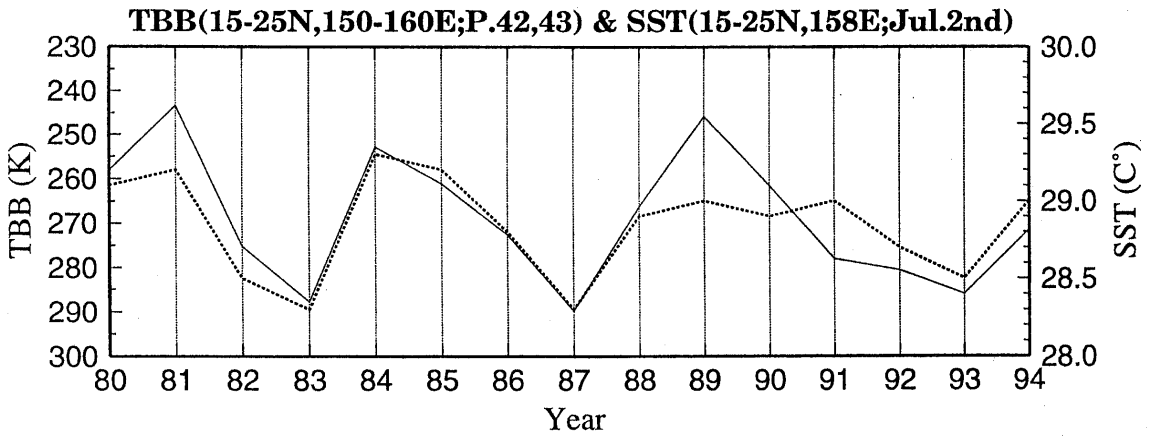

Fig. 4. Year-to-year variation of T_{BB} (solid line) during Pentads 42–43 in the key region and SST in middle July (dashed line) in the key region, averaged over 15°N–25°N, 158°E for the period from 1980 through 1994.

days or so, the unstable condition is gradually reduced through intensified convective activity associated with the jump.

5. Circulations

In the previous section, we have shown the strong association between SST in the half first of July and convection jump in late July. The evolution of SST in the key region occurs under the Pacific subtropical high system (Pacific high). In this section, we examine the role of the Pacific high in seasonal change of SST over the key region. In order to investigate the degree of extension and intensity of the Pacific high over the key region, we note the surface pressure field over the region around 20°N–30°N, 130°E–180°. Figure 7 depicts a longitude-time section of correlation coefficients between T_{BB} (i, P42–43) and $Z(i, P)$, where i represents interannual variation of geopotential height at 1000 hPa averaged between 20°N and 30°N and P denotes the pentad mean value. Positive (negative) correlation coefficients indicate that a negative (positive) anomaly of $Z(i, P)$ is correlated to active (inactive) convection of the key region in late July. In this diagram, a large negative correlation of less than -0.5 is seen at Pentad 36 (June 25–June 29) to the west of 150°E, which corresponds to extension of the western edge of the Pacific high (increase of geopotential height) due to active convection (decrease of T_{BB}) in late July. On the other hand, positive correlation (more than 0.5) is found at Pentad 36 between 155°E and 180°, indicating a weakening of the Pacific high, corresponding to active convection in late July. Another distinct positive correlation is noted at Pentads 42–43 between 130°E and 150°E, which may be related to the convection jump in late July.

To examine the difference between typical and atypical cases of the Pacific high in late June, the composites of 1000 hPa geopotential height and wind fields at Pentad 36 for (a) typical cases and (b) atypical cases are presented in Fig. 8. It is evident in the typical cases (Fig. 8a) that the Pacific high is dominated to the east of 150°E with anticyclonic circulation around the center of the Pacific high. The ridge extends in a northeast direction between 25°N–35°N from the key region to the center of the Pacific high, while a low geopotential height area with less than 70 gpm, probably corresponding to the Baiu trough, is identified over Japan, and the low-level southwesterly is clearly found between 20°N and 35°N to the south of Japan. It should be noted that the western edge of the Pacific high of the typical cases extends westward compared with the atypical cases (see Fig. 8b), which is consistent with the negative correlation in Fig. 7. The geopotential heights between 160°E and 180° along 20°N–30°N are lower than those of the atypical cases, which is in agreement with the results of the correlation analysis obtained from Fig. 7. A interesting feature of the wind fields in the typical cases is a weaker anticyclonic circulation around the western edge of the Pacific high around 20°N–30°N, 140°E–160°E than that of the atypical cases. In the composite anomalies of geopotential height and 1000 hPa wind fields between typical minus atypical cases (not shown), the above geopotential height patterns exhibit dipole structure along 25°N. Positive geopotential anomalies are seen to the south of Japan around 28°N, 140°E where a cut-off high is strengthened and an anticyclonic wind anomaly is evident. On the other hand, negative geopotential anomalies are observed in the typical cases around 30°N, 167°E, corresponding to a weakening of the Pacific high. It is important to emphasize that strong easterlies

NACSIS-Electronic Library Service

Meteorological Society of Japan

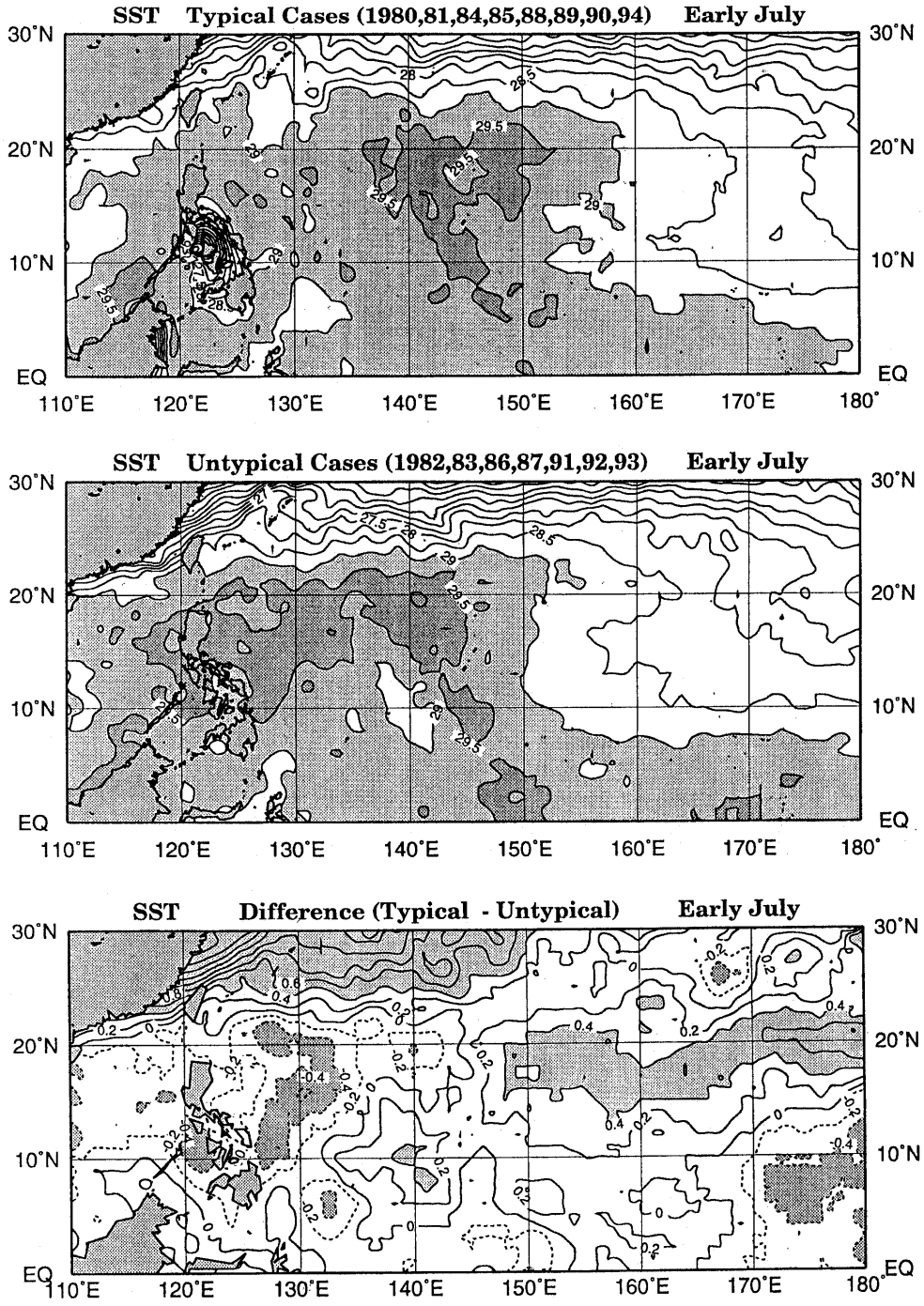

Fig. 5. Composited SST in early July for (a) typical cases, (b) atypical cases and (c) difference between typical cases and atypical cases. The contour interval is (a), (b) 0.5°C and (c) 0.2°C. Heavy shading denotes areas with SST (a), (b) more than 29.5°C and (c) less than −0.4°C, while light shading is for areas (a), (b) between 29.0°C and 29.5°C and (c) more than 0.4°C.

along 20°N are considerably reduced to the south of the ridge of the Pacific high.

Next, we examine the role of low-level wind velocity in producing an SST anomaly in the half first of July. Figure 9 shows a time-longitude section of correlation coefficients between the SST in early July in the key region and 1000 hPa wind velocity over the same latitude. Large negative correlation (less than −0.7) can be seen around 150°E at Pentad 36, which indicates that when the wind velocity in late June is weak (strong) then the following SST in early July increases (decreases).

NACSIS-Electronic Library Service

Meteorological Society of Japan

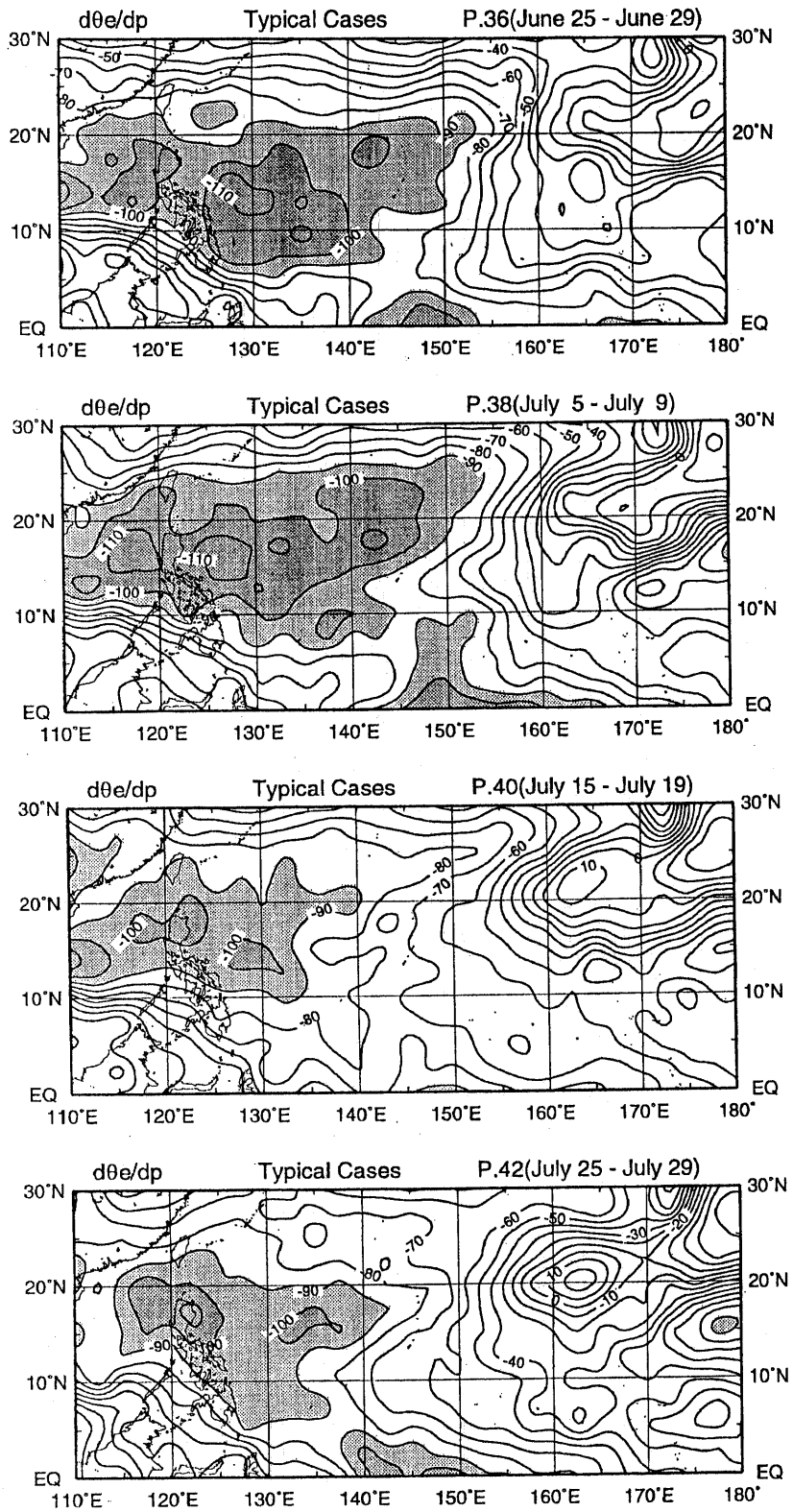

Fig. 6. Time evolution of gradient of equivalent potential temperature between 1000 hPa and 850 hPa for typical cases. (a) Pentad 36 (June 25–29), (b) Pentad 38 (July 5–9), (c) Pentad 40 (July 15–19) and (d) Pentad 42 (July 25–29). The contour interval is 10 $KhPa^{-1}$. Light (heavy) shading indicating regions of less than −90 (−100) $KhPa^{-1}$.

NACSIS-Electronic Library Service

Meteorological Society of Japan

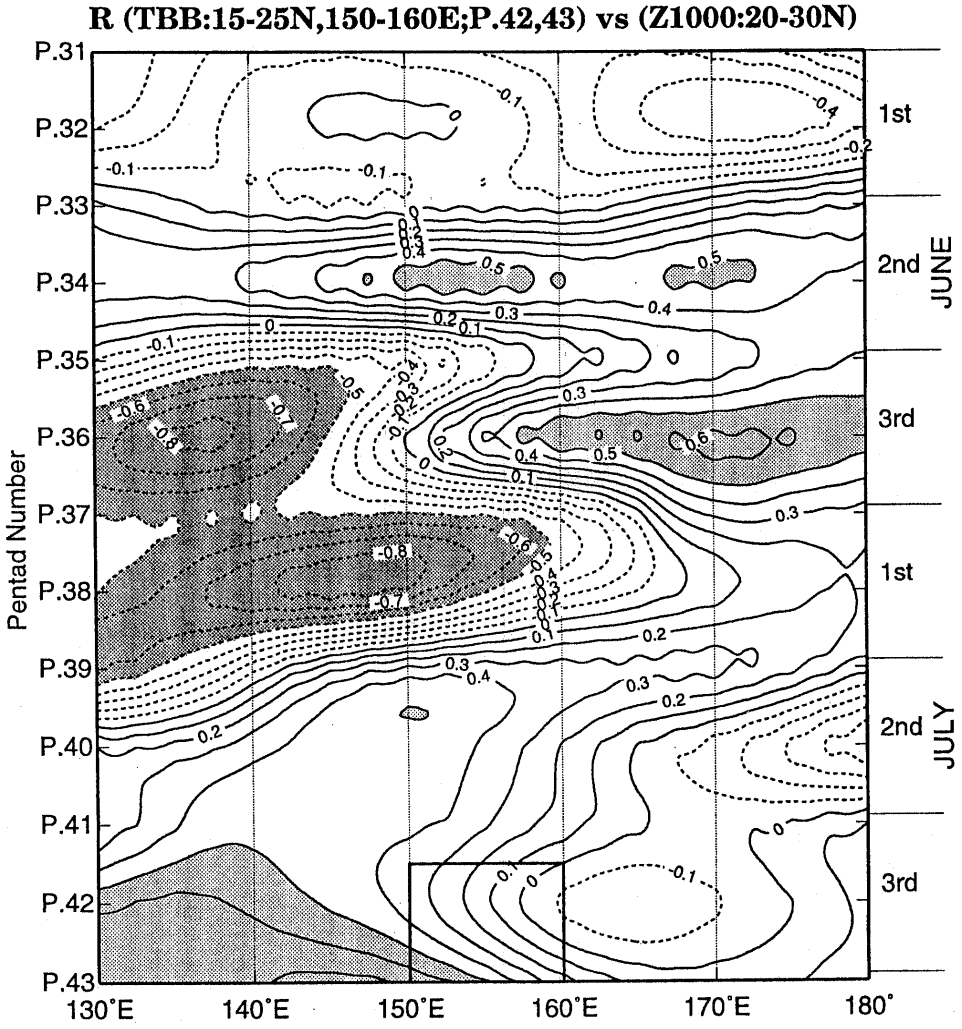

Fig. 7. Time-longitude sections of correlation coefficients between interannual variation of T_{BB} in the key region (15°N–25°N, 150°E–160°E) during Pentads 42, 43 (July 25–August 3) and interannual variation of geopotential height averaged over latitudes from 20°N through 30°N. The contour intervals are 0.1 and light (heavy) shading indicate correlation over 0.5 (below −0.5). The reference T_{BB} is denoted as a solid square.

In order to clarify the above relationships, the composite anomalies of 1000 hPa wind velocity at Pentad 36 for typical cases is presented in Fig. 10. In this figure, negative wind velocity anomalies are apparently seen over the region between 155°E and 175°E along 20°N and large negative wind velocity anomalies (less than-1 m/s) also exist between 20°N–30°N, 135°E–155°E. Compared with the configuration of the composite anomaly between the typical and the atypical cases of SST in early July (see Fig. 5c), one can notice that both positive SST anomalies exist over the region between 150°E and 180° along 20°N and 23°N–30°N, 130°E–150°E in excess of 0.4°C are consistent with the region of weak-wind velocity anomalies. In contrast, another interesting feature in Fig. 10 is the positive anomalies of the wind velocity to the east of the Philippine Islands around 15°E, 135°E, where negative SST anomalies are obvious in Fig. 5c. However, there still remains the problem that large negative anomalies of wind velocity over the mid-latitude region around 25°N, 145°E do not correspond to the key region. To confirm the above relationships between SST and low-level wind velocity, the spatial distribution of correlation coefficients between the SST in early July and the wind speed at 1000 hPa in late June is constructed in Fig. 11. Large negative correlations less than −0.7 are evident along 20°N between 148°E and 168°E. A further smaller area of negative correlation is seen around 25°N, 147°E. These results indicate that the weakening of easterlies along 20°N between 150°E and 170°E is

NACSIS-Electronic Library Service

Meteorological Society of Japan

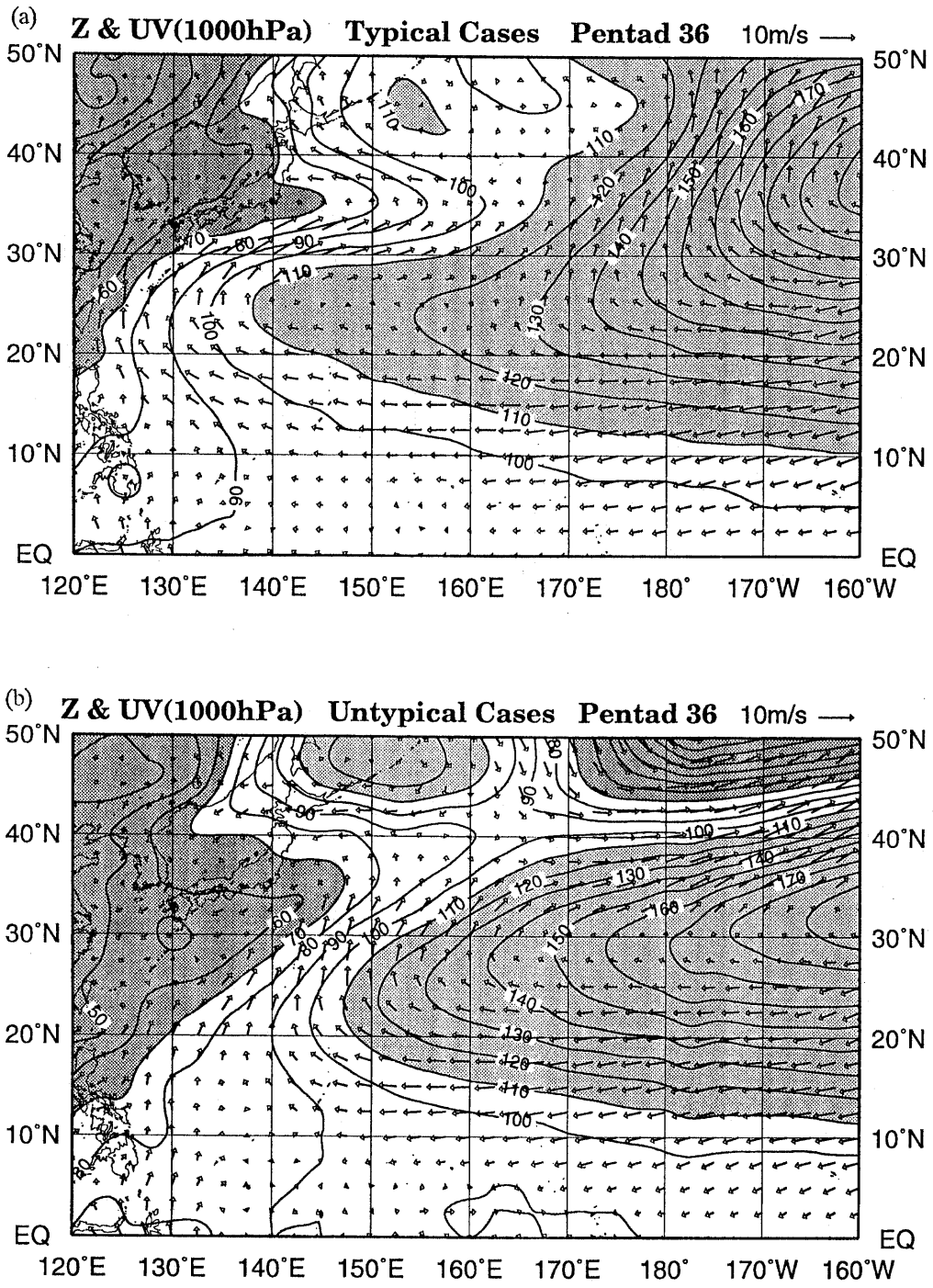

Fig. 8. Composite of geopotential height and wind fields at 1000 hPa at Pentad 36 (June 25–30) for (a) typical cases, (b) atypical cases. A 10 ms^{-1} reference vector is shown at the upper-right of this figure. Contours are drawn at every 10 gpm. Heavy shading denotes areas with less than 70 gpm, while light shading is for areas of more than 110 gpm.

the most important ingredient condition for a warming of the SST over the key region. The above results implies that when the wind velocity is weaker (stronger) than usual, then the SST increases (decreases) after 10 to 20 days later in this particular region, which is consistent with Kawamura (1988) and T. Murakami (1988).

In order to depict the relationships between the variation of the Pacific high and tropical western Pacific monsoon around middle June, the difference in T_{BB} and wind fields at 850 hPa for typical cases between Pentads 35–36 minus 32–33 is constructed

NACSIS-Electronic Library Service

Meteorological Society of Japan

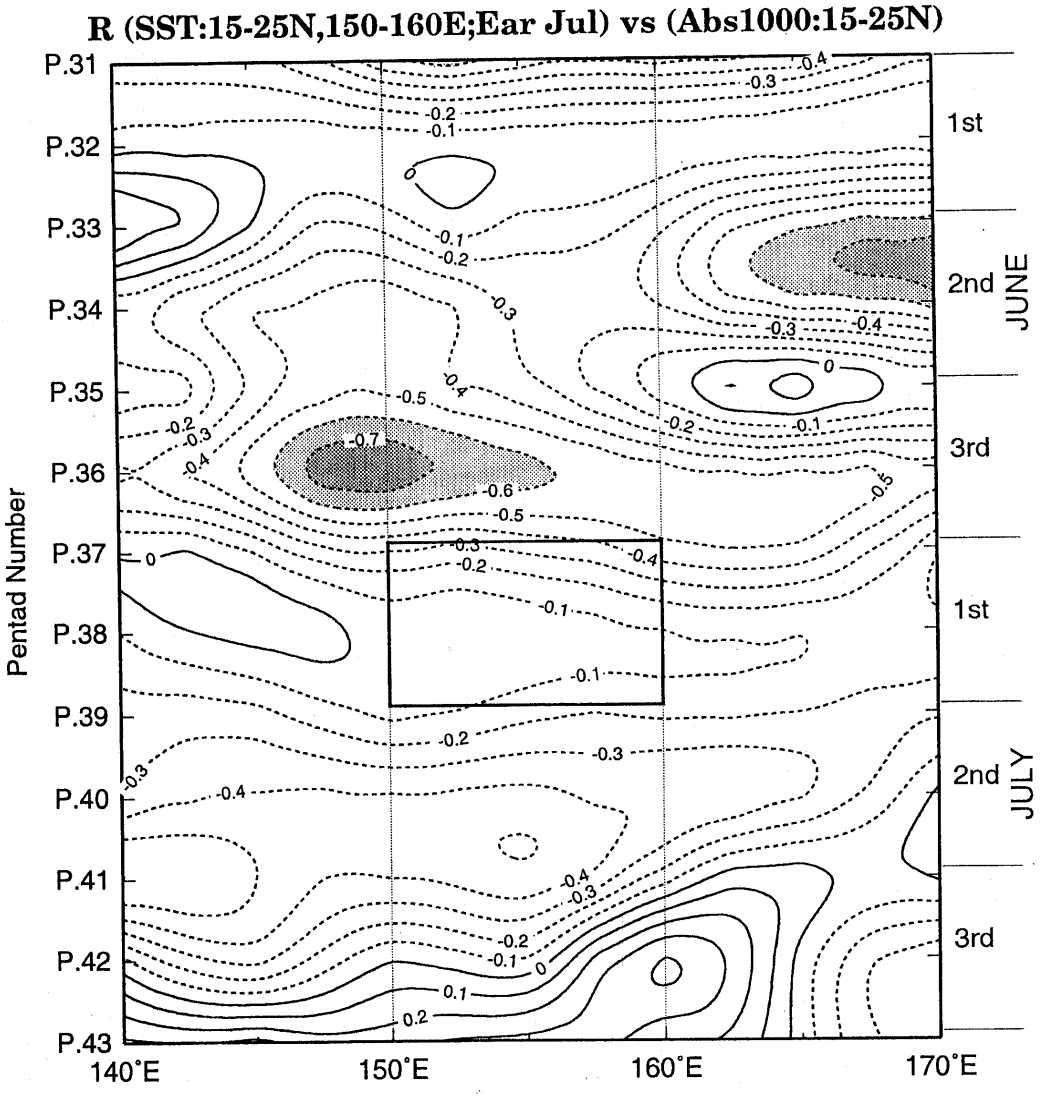

Fig. 9. Time-longitude sections of correlation coefficients between interannual variation of SST in the key region (15°N–25°N, 150°E–160°E) in early July and interannual variation of 1000 hPa wind velocity averaged over the same latitudes. Intervals are 0.1, with shading (dark shading) indicating regions of less than −0.6 (−0.7). The reference SST is drawn as a solid square.

in Fig. 12. Large negative anomalies (enhanced convection) are evident around the Philippine Islands with cyclonic wind anomalies. Further, anomalous cyclonic circulations are obvious over the western part of the Pacific high around 20°N–45°N, 150°E–170°W. However, there exist anticyclonic circulation anomalies between the above two cyclonic circulation anomalies which implies propagation of stationary Rossby waves induced by the onset of western Pacific monsoon. Nitta (1987) revealed that the propagation of Rossby waves is generated by a tropical heat source associated with active convection in the Philippine Sea during warm SST summers as identified by interannual variability. Quite recently, Kawamura *et al.* (1994) showed that this weakening of the Pacific high in late June is closely connected with the propagation of Rossby-like waves from the Philippines to around 40°N, 170°E with intraseasonal time scales. The above results indicate that SST warming in early July around 20°N, 150°E–180° is induced by the decrease of low-level wind velocity due to weakening of the western part of the Pacific high through reduction of both evaporative cooling and turbulent mixing of sea water. In addition, the westward extension of the western edge of the Pacific high induces warming of the SST due to an increase of solar radiation. Furthermore, this weakening of the western part of the Pacific high around 40°N, 170°E and the intensification of its western edge are closely related to the onset of the western Pacific monsoon around the Philippine Islands through the propagation of Rossby waves.

NACSIS-Electronic Library Service

Meteorological Society of Japan

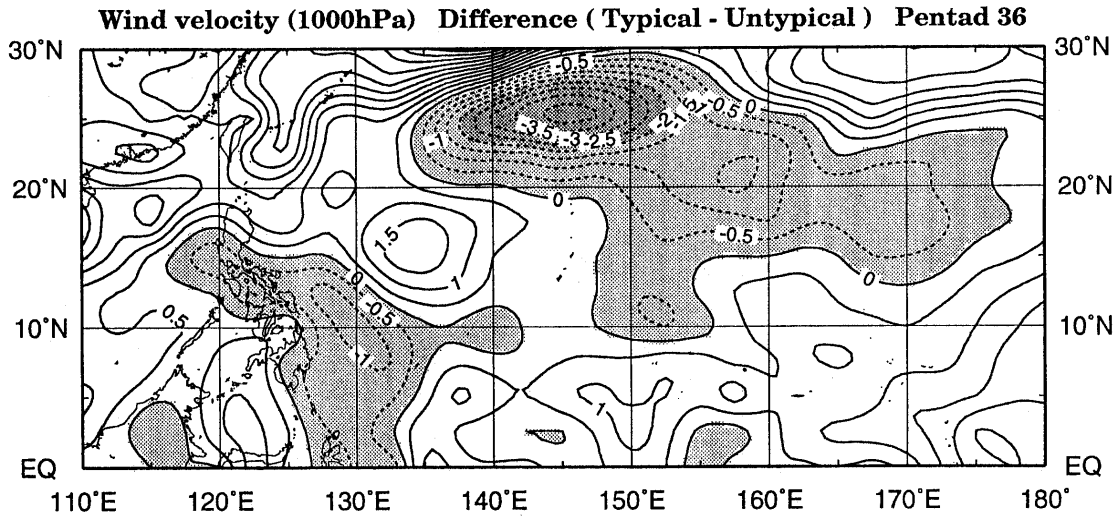

Fig. 10. Composite anomaly of 1000 hPa wind velocity between typical cases minus atypical cases at Pentad 36 (June 25–30). The contour interval is 0.5 ms^{-1}. Dark (light) shaded regions denote wind velocity of less than -2 ms^{-1} (between 0 and -2 ms^{-1}).

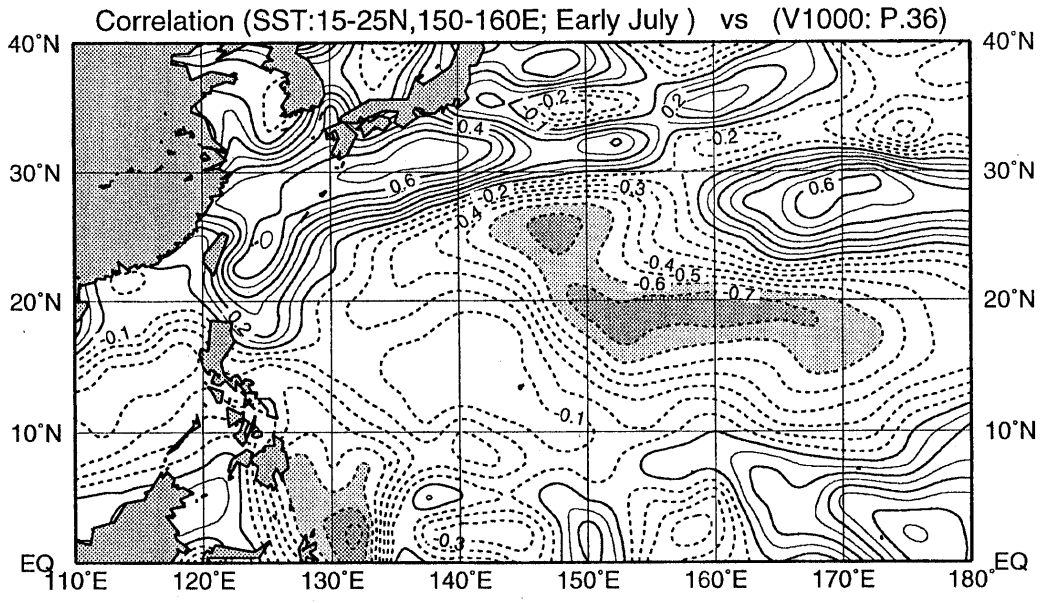

Fig. 11. Spatial distribution of correlation coefficients between interannual variation of SST in early July over the key region (15°N–25°N, 150°E–160°E) and interannual variation of wind velocity at 1000 hPa in late June (Pentad 36). Intervals are 0.1, with shading (dark shading) indicating regions of less than -0.6 (-0.7).

6. Discussion

Considering the above discussion, a schematic model of the maturing process of the summer monsoon over the western North Pacific for typical cases is proposed. The model shows the time evolution of the surface circulation field, including information on large-scale convective activity and SST over the subtropical western Pacific. The five stages of seasonal evolution are illustrated in Fig. 13 from early June to late July for typical cases.

Before early June (referred to as Stage A), the Pacific high is dominant to the west of 140°E. The center is located at 40°N, 150°W and the ridge line extends from the center to 20°N, 140°E. In the wind field, a strong trade wind (10°N–20°N) and monsoon southwesterlies prevailed around the Pa-

NACSIS-Electronic Library Service

Meteorological Society of Japan

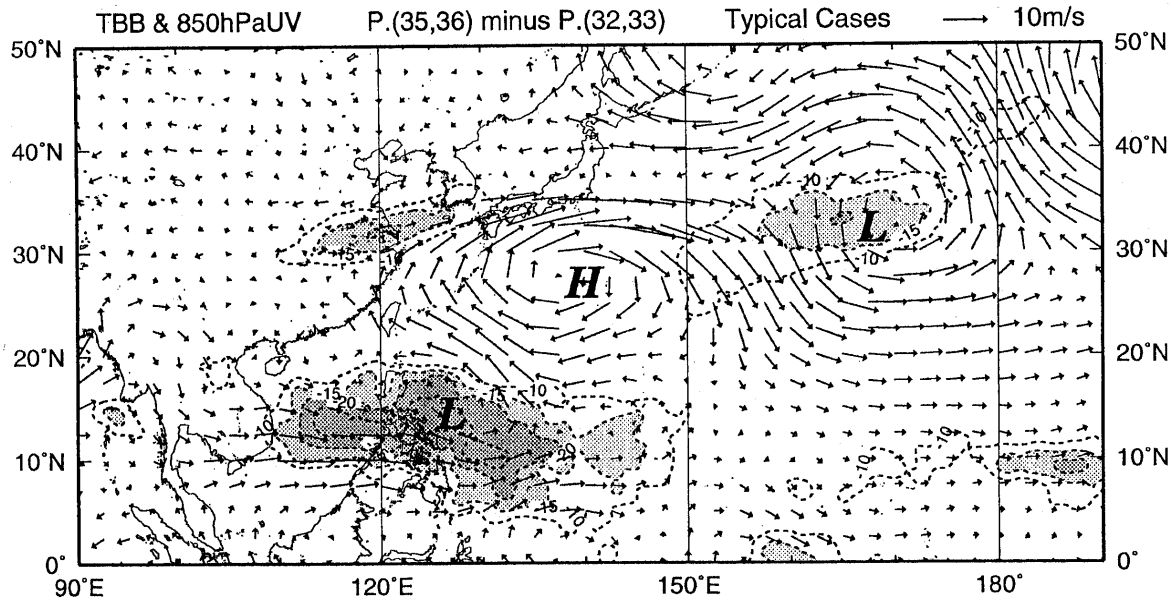

Fig. 12. Difference in T_{BB} and wind fields at 1000 hPa for typical cases between Pentads 35–36 minus Pentads 32–33. The unit vector is 10 ms^{-1} and the contour interval is 5 K, with shading (dark shading) indicating regions of less than −15 K (−20 K)

cific high. At Stage B, the western Pacific monsoon becomes most active around the Philippine Islands, where monsoon westerlies and easterlies merge forming cyclonic circulation. Associated with this active convection, the western part of the Pacific high between 150°E and 180° is abruptly weakened, while the western edge of the Pacific high is strengthened, due to the propagation of stationary Rossby waves. Accordingly, the trade wind is substantially reduced between 150°E and 180° along 20°N. A weak-wind region also appears around 20°N–30°N, 140°N–150°E, corresponding with the westward extension of the western edge of the Pacific high. In early July (Stage C), warming of the SST occurs over the weakened trade wind region along 20°N and east of 145°E (dotted line) producing the most unstable condition in the lower troposphere. Furthermore, incoming solar radiation along 20°N is strongest in this particular period of the season (*i.e.*, the summer solstice). At Stage D, the SST rises to its maximum of more than 29 °C over the key region (bold line). At Stage E, a jump of the convection occurs over 20°N, 150°E in late July as seen in T_{BB} field, which induces the propagation of a Rossby wave train, with a local high over and around Japan. This high pushes the Baiu front northward, bringing the withdrawal of the Baiu season around Japan.

Another important problem is the association between typical/atypical cases of the convection jump and El Niño events. Nitta (1986) showed that SST anomalies averaged over the tropical western Pacific (18°N–24°N, 158°E–166°E) in the Northern Hemisphere summer months (June–September) for the period of 1978–1988 are correlated with north-south oscillation patterns between the western Pacific near 20°N and the middle latitudes around 35°N (called SJ patterns). Moreover, most of cold anomalies of SST in the Philippine Sea are affected by El-Niño events exhibiting inactive convection (Nitta, 1987). In Fig. 4, an SST colder than 28.5°C is observed over the key region in the years 1983, 87, 89, which correspond with El-Niño years (U.S. Department of Commerce, 1996). The above results suggest that the interannual variation of the convection jump is not a local phenomenon but a part of the global-scale SST variability, probably related to El Niño, which is one of unresolved problems.

7. Concluding remarks

Through the analyses of T_{BB}, SST and circulation field, a mechanism for the convection jump over the western Pacific in late July has been discussed in the context of the maturing process of the summer monsoon. This process has been demonstrated to be a result of time-lag interaction among active convection in middle June around the Philippine Sea, the Pacific high circulation system, and the underlying ocean surfaces. These results are summarized as follows:

1) A typical convection jump in late July occurs in 8 years (1980, 1981, 1984, 1985, 1988, 1989, 1990, 1994) throughout the analysis period (1980 to 1994).

NACSIS-Electronic Library Service

Meteorological Society of Japan

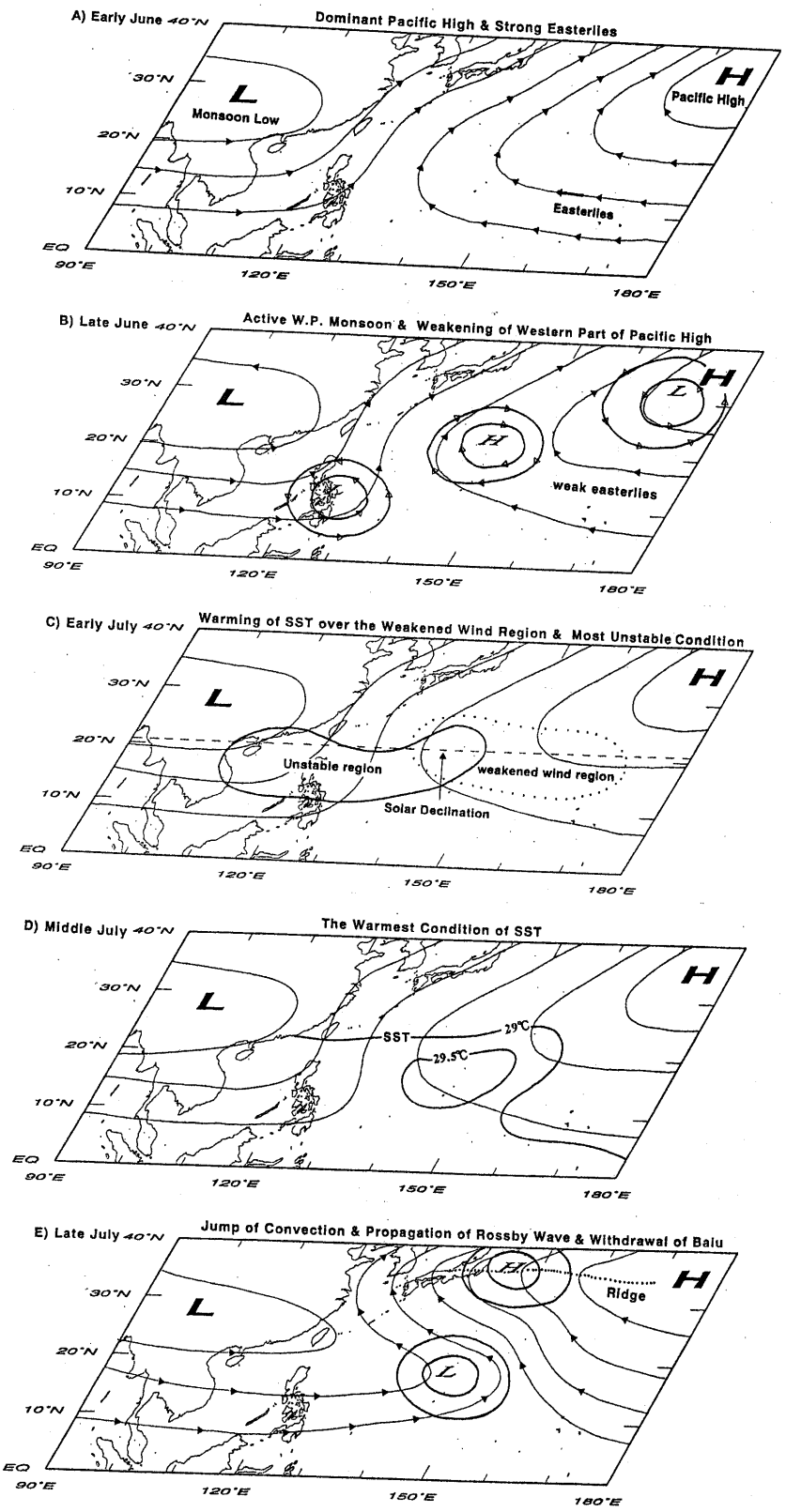

Fig. 13. Schematic illustration of the maturing process of summer monsoon over the western North Pacific for the period from early June (A) through late July (E).

NACSIS-Electronic Library Service

Meteorological Society of Japan

2) T_{BB} in late July over the key region (15°N–25°N, 150°E–160°E) is strongly correlated to SST during early to middle July over the same area. Furthermore, lag-correlation analysis between the above T_{BB} and 1000 hPa geopotential height fields shows that the intensity and extension of the Pacific high in late June is responsible for the inducing the convection jump.

3) Based on composite analyses of the convection jump and correlation analysis, the relation between the SST and circulation field is examined. In the typical cases, the SST in the early to middle July in the northeastern edge of its warm water pool (along 20°N to the east of 150°E) is warmer than that of atypical cases. Before the warming of SST, the western part of the Pacific high in late June is considerably weakened, while the western edge of the Pacific high is strengthened.

4) This behavior of the Pacific high seems to be induced by the propagation of Rossby waves excited by enhanced convection near the Philippine Islands.

5) The SST in early July over the key region is well correlated to surface wind velocity over the key region in late June, which implies that when the wind speed is weaker (stronger) than usual then the SST increases (decreases).

6) This weak-wind region in late June, in turn, is likely to be responsible for the warming of the SST due to a decrease of evaporative cooling and turbulent mixing of sea water, as well as a summer solstice condition of insolation.

7) During the period from the warming of the SST in early July to the convection jump in late July, the atmosphere gradually becomes unstable in early July over the key region which, as a consequence, abruptly induces strong convective activity manifested as a convection jump.

This study has revealed the seasonal evolution of the summer monsoon between the active western Pacific monsoon in middle June and the abrupt convection jump in late July. However, the onset and maintenance mechanisms of the western Pacific monsoon during June need to be investigated as part of the large-scale Asian summer monsoon. The interannual modulation of the convection jump and its relationship to El Niño is another issue to be further examined.

Acknowledgments

The authors wish to thank Dr. Ryuichi Kawamura of National Research Institute for Earth Science and Disaster Prevention for his constant encouragement and helpful advice throughout this work. They would also like to express their sincere appreciation to the two anonymous reviewers for many valuable comments during the course of completing this work. Special thanks are due to Mr. Kazuo Kimura of Hamagin Research Institute, Ltd. for his interest and suggestions. The authors also thank Dr. Tetsuo Nakazawa of the Meteorological Research Institute for providing them with T_{BB} data from a GMS satellite. This research was also partly supported by a Grant-in-Aid for Scientific Research by the Ministry of Education Science and Culture.

References

Gadgil, S., P.V. Joseph and N.V. Joshi, 1984: Ocean-atmosphere coupling over monsoon regions. *Nature*, **312**, 141–143.

Kawamura, R., 1988: Intraseasonal variability of sea surface temperature over the tropical western Pacific. *J. Meteor. Soc. Japan*, **66**, 1007–1012.

Kawamura, R., T. Yasunari and H. Ueda, 1994: Abrupt changes of seasonal evolution of large-scale convective activity and tropical cyclone over the western Pacific. *Report of the National Research Institute for Earth Science and Disaster Prevention*, **53**, 1–18 (in Japanese with English Abstract).

Kawamura, R., M. Sugi and N. Sato, 1994: A modeling study of the summer monsoon variability over the east Asia and the western Pacific. *Proceeding of the International Conference on Monsoon Variability and Prediction*, Italy, 789–795.

Matsumoto, J., 1989: The seasonal changes of tropical cloud distribution as revealed from 5-day mean outgoing longwave radiation. *Bull. Dept. Geogr. Univ. Tokyo*, **21**, 19–35.

Matsumoto, J., 1990: The seasonal changes of wind fields in the global tropics. *Geogr. Rev. Japan, (Ser. B)*, **63**, 156–178.

Matsumoto, J., 1992: The seasonal changes in Asian and Australian monsoon regions. *J. Meteor. Soc. Japan*, **70**, 257–273.

Murakami, T., 1988: Relationships between sea surface temperature and outgoing longwave radiation on intraseasonal time scales. *Tenki*, **35**, 715–721 (in Japanese).

Murakami, T. and J. Matsumoto, 1994: Summer monsoon over the Asian continent and western North Pacific. *J. Meteor. Soc. Japan*, **72**, 719–745.

Nakazawa, T., 1992: Seasonal phase lock of intraseasonal variation during the Asian summer monsoon. *J. Meteor. Soc. Japan*, **70**, 597–611.

Nitta, Ts., 1986: Long-term variations of cloud amount in the western Pacific region. *J. Meteor. Soc., Japan*, **64**, 373–390.

Nitta, Ts., 1987: Convective activities in the tropical western Pacific and their impact on the Northern Hemisphere summer circulation. *J. Meteor. Soc., Japan*, **65**, 373–390.

Tanaka, M., 1992: Intraseasonal oscillation and the onset and retreat dates of the summer monsoon over

NACSIS-Electronic Library Service

Meteorological Society of Japan

East, Southeast Asia and the western Pacific region using GMS high cloud amount data. *J. Meteor. Soc. Japan*, **70**, 613–6 29.

Ueda, H., T. Yasunari and R. Kawamura, 1995: Abrupt seasonal change of large-scale convective activity over the western Pacific in the northern summer. *J. Meteor. Soc. Japan*, **73**, 795–809.

U.S. Department of Commerce National Oceanic and Atmosphere Administration, 1996: *Climate Diagnostics Bulletin, April 1996*, 11pp.

西部北太平洋上における夏季モンスーンの成熟過程ー大気海洋結合系ー

植田宏昭
（筑波大学地球科学研究科）
安成哲三
（筑波大学地球科学系）

西部北太平洋域の夏季モンスーン季節変化に見られる10°N, 150°E付近にあった対流活発域が、7月25–29日（第42半旬）ころに急激に北上する（対流ジャンプ）現象と先行する現象について、等価黒体温度（TBB）および海面水温（SST）データ（1980–1994年）と循環場データ（1980–1989）を用いて調べた。

6月中旬から7月中旬の間の夏のモンスーンの成熟過程のメカニズムを、顕著な対流ジャンプの見られた8年（典型例）のとそれ以外の7年（非典型例）を比較しながら調べた。典型的なジャンプに先行して、SST高温域（29°C以上）は7月の上旬に20°N, 150–160°E付近に舌状に広がる。このSST上昇は、6月の下旬に25N, 140–160付近に出現する弱風域（偏東風の弱体化）に密接に関係している。この弱い偏東風は、6月の中下旬にフィリピン付近で活発化する対流活動によって励起されるロスビー波の伝播と結び付いていることが示唆される。また、非典型年はエルニーニョが起こっている時期にあたることが多い。

NACSIS-Electronic Library Service